Ocean Modelling 187 (2024) 102308

Contents lists available at ScienceDirect

Ocean Modelling

journal homepage: www.elsevier.com/locate/ocemod

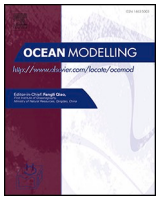

Description of FIO-ESM version 2.1 and evaluation of its sea ice simulations

Qi Shu [a,b,c], Fangli Qiao [a,b,c], Jiping Liu [d], Ying Bao [a,b,c], Zhenya Song [a,b,c,*]

[a] First Institute of Oceanography and Key Laboratory of Marine Science and Numerical Modeling, Ministry of Natural Resources, Qingdao 266061, China
[b] Laoshan Laboratory, Qingdao 266237, China
[c] Shandong Key Laboratory of Marine Science and Numerical Modeling, Qingdao 266061, China
[d] School of Atmospheric Sciences, Sun Yat–sen University, Zhuhai 519082, China

ARTICLE INFO

Keywords:
FIO-ESM
Climate Model
Ice–ocean heat exchange parameterization
Sea ice extent

ABSTRACT

To improve Arctic sea ice simulations by the First Institute of Oceanography–Earth System Model (FIO–ESM), the model version has been updated from FIO–ESM v2.0 to FIO–ESM v2.1 by upgrading its sea ice component from Los Alamos Sea–Ice Model (CICE) version 4.0 (CICE4.0) to CICE6.0, and improving the ice–ocean heat exchange process from a two–equation boundary condition parameterization to a more realistic three–equation boundary condition parameterization. Numerical experiments show that the underestimation of Arctic summer sea ice extent (SIE) in FIO–ESM v2.0 is significantly improved by the model enhancements. The root mean square error of the simulated Arctic September SIE during 1979–2014 is reduced from 2.9 million to 0.7 million km^2. Nevertheless, the biases of Antarctic SIE increase following the model version update. FIO–ESM v2.1 performs well for the simulations of surface air temperature, sea surface temperature, Atlantic Meridional Overturning Circulation, and Arctic SIE; however, it overestimates summer SIE in the Antarctic. Furthermore, future projections based on FIO–ESM v2.1 indicate that the first ice–free Arctic summer will occur in the 2050s and the 2040s under SSP2–4.5 and SSP5–8.5, respectively.

1. Introduction

Climate models are the primary tools available for investigating Earth climate system response to various forcings, making climate predictions on seasonal to decadal timescales, in addition to making projections over the coming century and beyond (IPCC, 2014). Climate models have been developed from relatively simple atmosphere–ocean coupled models to highly sophisticated Earth system models. However, even state–of–the–art climate models suffer from systematic biases, substantial inter–model spreads, and large levels of uncertainty (IPCC, 2014). Accordingly, improving the model physical processes based on new understandings of climate represents one effective way of addressing these issues.

The First Institute of Oceanography–Earth System Model version 1.0 (FIO–ESM v1.0) is the first climate model to incorporate an ocean surface wave model by considering the processes of non–breaking surface wave–induced ocean vertical mixing (Qiao et al., 2013, 2004). FIO–ESM v2.0 is the updated version of FIO–ESM v1.0 by upgrading atmospheric and land component models, improving model resolution, and including some novel physical processes, such as the effects of surface wave Stokes drifts on air–sea momentum and heat fluxes, wave–induced sea spray on air–sea sensible and latent heat fluxes, as well as that of sea surface temperature (SST) diurnal cycles on air–sea sensible heat flux (Bao et al., 2020). FIO–ESM v2.0 participated in the Climate Model Intercomparison Project phase 6 (CMIP6), and reproduces the surface air temperature (SAT), precipitation, SST, Atlantic Meridional Overturning Circulation (AMOC), El Niño–Southern Oscillation (ENSO), significant wave height, and other climatological indices of interest well (Bao et al., 2020; Lee et al., 2021; Song et al., 2020, 2022; Zhang et al., 2022). However, FIO–ESM v2.0 underestimates the Arctic summer sea ice extent (SIE; Shu et al., 2022, 2020).

Arctic sea ice is a particularly important component of Earth's climate system, while Arctic sea ice concentration and extent have declined markedly across all regions and seasons throughout the satellite era (Onarheim et al., 2018; Stroeve and Notz, 2018). These changes have potential dramatic effects on the Arctic marine ecosystem, Northern Hemisphere weather, mid– and high-latitude climates, as well as the navigability of trans–Arctic shipping (Lannuzel et al., 2020; Min et al., 2022; Mori et al., 2014; Sévellec et al., 2017). Therefore, the primary aim of the present study is to improve Arctic sea ice simulations by

* Corresponding author at: First Institute of Oceanography and Key Laboratory of Marine Science and Numerical Modeling, Ministry of Natural Resources, Qingdao 266061, China.
E-mail address: songroy@fio.org.cn (Z. Song).

https://doi.org/10.1016/j.ocemod.2023.102308
Received 9 August 2023; Received in revised form 26 October 2023; Accepted 17 December 2023
Available online 18 December 2023

FIO–ESM.

To this end, FIO–ESM v2.0 is updated here to FIO–ESM v2.1 by upgrading the sea ice component model from Los Alamos Sea–Ice Model (CICE) version 4.0 (CICE4.0; Hunke and Lipscomb, 2010) to CICE6.0 (Duvivier, 2018), and improving the physical process of ice–ocean heat exchange from a two–equation boundary condition (2EQ) parameterization to a more realistic three–equation boundary condition (3EQ) parameterization (Shi et al., 2021; Yu et al., 2022), respectively. In this study, the influences of the sea ice component model upgrade and 3EQ parameterization on sea ice simulations by FIO–ESM v2.1 are investigated, the performances of FIO–ESM v2.1 are evaluated, the improvements over FIO–ESM v2.0 are studied, and future sea ice projections by FIO–ESM v2.1 are demonstrated. The remainder of the paper is organized as follows: FIO–ESM v2.1 is introduced and the numerical experimental design is described in Section 2. Section 3 presents the results of the numerical experiments, while the conclusions and discussion are presented in Section 4.

2. Model description and numerical experimental design

2.1. Description of FIO–ESM v2.1

Fig. 1 presents the framework of FIO–ESM v2.1. The five component models, including the atmospheric general circulation model (AGCM), land surface model, ocean general circulation model (OGCM), ocean surface wave model, and sea ice model, represent the physical component models of FIO–ESM v2.1. These models refer to the Community Atmosphere Model version 5 (CAM5; Neale et al., 2012), Community Land Model version 4.0 (CLM4; Lawrence et al., 2011), Parallel Ocean Program (POP2; Smith et al., 2010), MASNUM surface wave model (Qiao et al., 2016), and CICE6.0 (Duvivier, 2018), respectively. All component models are coupled by a coupler (CPL7) in FIO–ESM v2.1. The horizontal resolutions of CAM5 and CLM4 are 1.25° longitude × 0.9° latitude, whereas those of POP2, MANSUM surface wave model, and CICE6.0 have resolutions of approximately 1.1° longitude × 0.27–0.54° latitude. The number of vertical layers in CAM5 and POP2 are 30 and 61, respectively. CAM5, CLM4, and CICE6.0 exchange data with the coupler every 30 min, while the POP2 and MANSUM surface wave models exchange data with the coupler at 3–h intervals.

The primary difference between FIO–ESM v2.0 and v2.1 is the upgraded sea ice component model from CICE4.0 to CICE6.0. CICE is a thermodynamic–dynamic sea–ice model developed by the Los Alamos National Laboratory. The default Bitz and Lipscomb thermodynamic model (Bitz and Lipscomb, 1999) in CICE4.0 is replaced by a new mushy–layer thermodynamics model (Turner and Hunke, 2015) in CICE6.0. Additionally, several parameterizations, such as melt pond, form drag, and snow ice formation are also improved in CICE6.0.

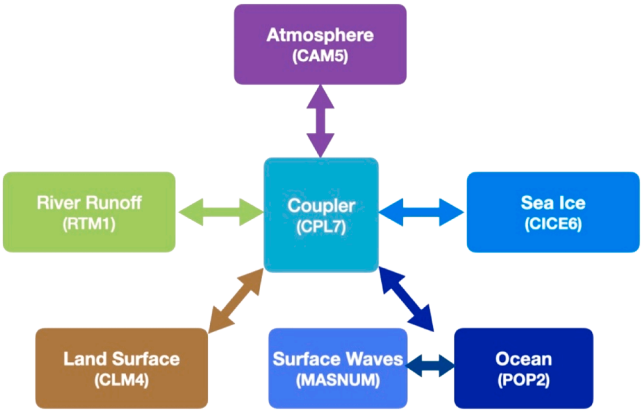

Fig. 1. FIO–ESM v2.1 framework: The sea ice component model is upgraded from CICE4.0 (FIO–ESM v2.0) to CICE6.0, and the ice–ocean heat exchange parameterization is improved from a two–equation parameterization to a more realistic three–equation boundary condition parameterization.

Furthermore, the physical process of ice–ocean heat exchange is improved in FIO–ESM v2.1 from the default 2EQ parameterization in CICE6.0 to a more realistic 3EQ parameterization. Both the 2EQ and 3EQ parameterizations treat the oceanic heat flux at the ice–ocean interface as turbulent, with their values dependent upon the temperature differences between the underlying ocean and the ice–ocean interface. The difference between these two parameterizations centers around their calculation of the ice–ocean interface temperature (Shi et al., 2021; Yu et al., 2022): In the 2EQ parameterization, the ice–ocean interface temperature is maintained at the freezing temperature of seawater (as calculated based on the mixed layer salinity); whereas in the 3EQ parametrization, the ice–ocean interface temperature is calculated based on the local salinity (interfacial salinity) set by the ice ablation rate. Although the 2EQ parameterization is relatively simple and has been widely used in sea ice models, it results in too fast salt flux exchanges between the ice–ocean interface and mixed layer. Accordingly, appropriate consideration of the slower salt transfer rate than that of heat mandates that the mixed–layer salinity should be replaced with the actual interfacial salinity to better represent the ice–ocean heat flux. Therefore, compared to the 2EQ parameterization, the 3EQ parameterization includes an additional salinity balance equation to explicitly calculate the interface salinity (Shi et al., 2021; Yu et al., 2022). This more realistic 3EQ boundary condition induces a fresher ice–ocean interface in the melting season, causing less oceanic heat to melt sea ice (Yu et al., 2022), and thus potentially improving the underestimation of summer sea ice by the models with the 2EQ parameterization. Here, the 3EQ parameterization has been embedded in FIO–ESM v2.1 and set to the default ice–ocean heat flux parameterization scheme. Further details regarding these two parameterizations have been described in previous studies (Shi et al., 2021; Yu et al., 2022).

2.2. Numerical experimental design

To investigate the influence of the 3EQ boundary condition parameterization on sea ice simulation under FIO–ESM v2.1, two numerical experiments (*2EQ* and *3EQ*) are conducted (Table 1). The initial conditions of the AGCM, OGCM, ocean surface wave model, and land surface model for the two numerical experiments are obtained from the restart files of the 1950 FIO–ESM v2.0 CMIP6 *Historical* run, while those of the sea ice model are obtained from a standalone CICE6.0 run. By comparing the simulation results of Experiments *2EQ* and *3EQ* from 1950–2014, the role of the 3EQ boundary condition parameterization can be better quantified. The effects of sea ice component model upgrade can be studied by comparing the simulation results of the FIO–ESM v2.1 *2EQ* experiment and FIO–ESM v2.0 *Historical* experiment.

To further evaluate the improvements under FIO–ESM v2.1, a *Historical* numerical simulation is conducted (Table 1) from 1850 to 2014.

Table 1
Numerical experimental design.

Experiment name	Boundary condition parameterization	Simulation period (Start–End year)	Motivation
2EQ	2EQ	1950–2014	Sensitive experiments for influences of 2EQ and 3EQ
3EQ	3EQ	1950–2014	
Historical	3EQ	1850–2014	Evaluation of the FIO–ESM v2.1 simulation performances
SSP1–2.6	3EQ	2015–2100	
SSP2–4.5	3EQ	2015–2100	
SSP5–8.5	3EQ	2015–2100	

The initial conditions of the AGCM, OGCM, ocean surface wave model, and land surface model are identical to those of the FIO–ESM v2.0 CMIP6 *Historical* run (obtained from the FIO–ESM v2.0 CMIP6 *PiControl* simulation). The *Historical* simulations of FIO–ESM v2.0 and FIO–ESM v2.1 are the same but use different model versions. Therefore, we can study the performances of FIO–ESM v2.1 and the improvements from FIO–ESM v2.0 to FIO–ESM v2.1 by comparing their *Historical* simulation results to the observations or reanalysis datasets.

To demonstrate the Arctic and Antarctic sea ice projections using FIO–ESM v2.1, three scenarios are simulated—Shared Socioeconomic Pathway 1–2.6 (*SSP1–2.6*), *SSP2–4.5*, and *SSP5–8.5*—representing the low, medium, and high ends of future forcing pathways (O'Neill et al., 2016; Riahi et al., 2017), equating to effective radiative forcings of 2.6, 4.5, and 8.5 $W{\cdot}m^{-2}$ in 2100, respectively. Based on the multi–model ensemble mean results of CMIP6 Scenario Model Intercomparison Project, the global mean SAT anomalies from 2081 to 2100 under the three scenarios are 1.23°C, 2.14°C, and 3.99°C relative to the historical baseline of 1995–2014 (Tebaldi et al., 2021), respectively. Here, the future scenario experiment simulations from 2015 to 2100 are continuous runs of the FIO–ESM v2.1 *Historical* experiment, but with scenario external forcing.

For all experiments above, the external forcings are prescribed to the observation or scenario forcing data provided by CMIP6 (Eyring et al., 2016) available at https://esgf–node.llnl.gov/search/input4mips/. Details on incorporating external forcings into FIO–ESM are described in Bao et al. (2020).

In this study, the global ocean–ice coupled simulations forced by reanalysis forcing, such as OMIP (Ocean Model Intercomparison Project) experiments (Griffies et al., 2016), were not conducted. Because the sea surface salinity restoring is necessary for global ocean–ice coupled simulation to prevent climate drifts. The salinity restoring will lead to nonphysical negative feedback (Griffies et al., 2009), which may affect the interface salinity calculation in the 3EQ boundary condition parameterization.

3. Results

3.1. Effects of sea ice component model upgrade

Fig. 2 shows the climatological Arctic and Antarctic SIE during 1979–2014 based on satellite observations, FIO–ESM simulations, and CMIP6 multi-model mean results. The Arctic produced maximum and minimum values in March and September, respectively. The winter SIE simulated by the FIO–ESM fits the observations well. The main bias in Arctic sea ice simulations by FIO–ESM v2.0 is the underestimation of summer and especially September SIE (Fig. 2a). The satellite–observed Arctic SIE in September throughout 1979–2014 is 6.3 million km^2, while the simulated FIO–ESM v2.0 value is 3.4 million km^2. The root mean square error (RMSE) of simulated Arctic September SIE is 2.9 million km^2. The simulations of Arctic summer SIE is significantly improved by sea ice component model upgrade, where the September SIE value under the *2EQ* experiment is 5.2 million km^2. The RMSE is reduced to 1.3 million km^2.

Satellite observations show that the Antarctic SIE has the maximum and minimum values in September and February, respectively. FIO–ESM v2.0 does well to reproduce the seasonal cycles over this region (Fig. 2b). Compared to FIO–ESM v2.0, FIO-ESM v2.1 (*2EQ* experiment) reproduces a larger Antarctic SIE, especially in austral summer (February and March). Considering the relatively good performances of Antarctic summer SIE simulations in FIO–ESM v2.0, simulation biases of Antarctic sea ice are increased after upgrading the sea ice component model.

Differences between the FIO–ESM v2.0 and v2.1 *2EQ* experiments are caused by the sea ice component model upgrade. The responses of SIE in the Arctic and Antarctic to upgrading the sea ice model from CICE4.0 to CICE6.0 are similar, i.e., more summer sea ice by CICE6.0. Therefore, the underestimation of summer Arctic sea ice in FIO–ESM has been improved by the CICE upgrade. A previous study based on sea ice standalone sea ice models also demonstrates that the underestimated Arctic summer sea ice simulated by CICE4.0 can be improved by CICE6.0 (Wang et al., 2020). However, several parameterizations are improved upon between CICE4.0 and CICE6.0, and numerous default model parameters also differ between the two versions as well; therefore, it is difficult to determine precisely which parameterizations or parameters caused the differences.

3.2. Effects of 3EQ boundary condition parameterization

Fig. 2a shows that further improvements in Arctic summer SIE are achieved under the FIO–ESM v2.1 *3EQ* experiment by implementing 3EQ parameterization. The SIE in the *3EQ* experiments is 6.1 million km^2, and the RMSE is 0.7 million km^2, respectively. The RMSE of FIO–ESM v2.1 with 3EQ parameterization is close to that (0.6 million km^2) of the multi-model mean of 33 CMIP6 climate models.

Based on standalone sea ice model simulations (Yu et al., 2022), the 3EQ parameterization simulates lower interface salinity during the summer months, resulting in a higher ice–ocean freezing temperature

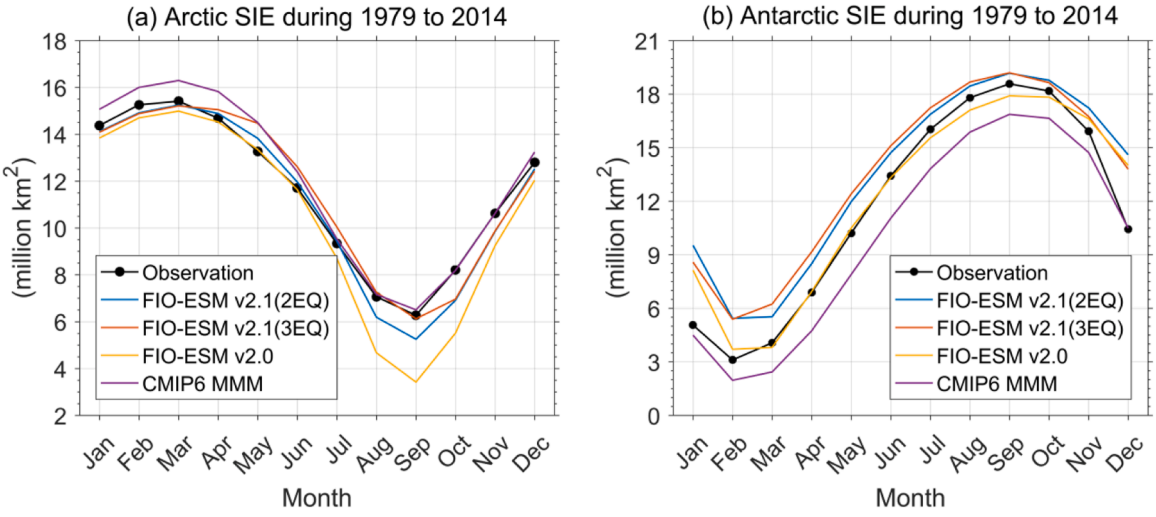

Fig. 2. (a) Arctic and (b) Antarctic climatological sea ice extent (SIE) during 1979–2014 based on satellite observations (Fetterer et al., 2017), FIO–ESM simulations, and CMIP6 multi-model mean (MMM) results.

(interface temperature), thereby reducing the upward oceanic heat flux and slowing the basal melt rate. Mixed layer salinity and ice–ocean interface salinity are used to calculate the ice–ocean interface temperature by 2EQ and 3EQ parameterizations, respectively. Fig. 3 shows that the ice–ocean interface salinity simulated by the 3EQ parameterization in the fully coupled model is also lower than mixed layer salinity simulated by the 2EQ parameterization in August. The reduction in boreal summer ice–ocean net heat exchanges in the fully coupled experiments here is also well represented (Fig. 4), resulting in higher summer sea ice concentrations and SIE (Figs. 2 and 5). Therefore, this indicates that the underestimated Arctic summer SIE by climate models with the 2EQ boundary condition can be improved by the 3EQ boundary condition in the fully coupled models.

Fig. 2b depicts the relatively small differences in Antarctic SIE between the *2EQ* and *3EQ* simulations. Similar results have also been reported by Shi et al. (2021). We checked the ice–ocean net heat exchanges and sea ice concentration responses to the change in ice–ocean heat exchange parameterizations. Although the SIE difference is small, Antarctic ice–ocean net heat exchanges are also reduced and the sea ice concentration is increased in most regions in austral summer by replacing the 2EQ parameterization with the 3EQ parameterization (Figs. 6 and 7), similar to the responses in the Arctic (Figs. 4 and 5).

3.3. Historical simulation comparisons between FIO–ESM v2.0 and v2.1

In this section, *Historical* experiments simulated SAT, SST, AMOC, and sea ice concentration and thickness under FIO–ESM v2.0 and v2.1 are compared with the analysis/reanalysis datasets or observations to evaluate the model performance and improvements.

Anomalies in the simulated global mean SAT and SST relative to 1961–1990 are compared with the HadCRUT analysis (Morice et al., 2021) and ERSSTv5 observations (Huang et al., 2017), respectively. Global mean SAT and SST anomalies have no large differences between FIO–ESM v2.0 and v2.1 (Fig. 8), as both models fit the analysis and observation values relatively well. It indicates that FIO–ESM v2.0 and FIO–ESM v2.1 can successfully reproduce the warming trends of SATs and SSTs over the past century.

The SAT and SST differences between FIO–ESM v2.0 and v2.1, are primarily limited to high–latitude regions (Fig. 9). Compared with the National Centers for Environmental Prediction–US Department of Energy reanalysis 2 (NCEP–DOE reanalysis 2; Kanamitsu et al., 2002), FIO–ESM v2.0 over– and underestimates SATs in the Arctic and Antarctic regions, respectively (Fig. 9a). By updating the sea ice component model and improving the ice–ocean heat exchange parameterization, SATs over the polar regions are lower in FIO–ESM v2.1 (Fig. 9 b and c), thereby reducing warm biases in the Arctic, but increasing cold biases in the Antarctic. Similarly, SST over high–latitude oceans also decreases from FIO–ESM v2.0 to v2.1 (Fig. 9f); however, the difference is relatively small. Comparatively, warmer SST is simulated in the North Atlantic Ocean by FIO–ESM v2.1 (Fig. 9f), which is mainly due to the changes in the AMOC, thus reducing the cold biases in FIO–ESM v2.0. In general, both FIO–ESM v2.0 and v2.1 perform well for SAT and SST simulations (Fig. 9a, b, d, and e).

The AMOC is an important regulator of global climate systems. Here, the FIO–ESM simulated AMOC strengths are compared with observations from the Rapid Climate Change–Meridional Overturning Circulation and Heat Flux Array–Western Boundary Time Series (RAPID/MOCHA; Moat et al., 2022). The AMOC strength (index) is defined as the maximum overturning stream function at 26.5° N in the Atlantic Ocean (Weijer et al., 2020). The average RAPID/MOCHA observed AMOC index is 17.69 ± 1.67 Sv during 2004–2014; whereas FIO–ESM v2.0 and v2.1 simulate values of 18.35 and 18.99 Sv over the same period (Fig. 10). Compared to the 27 CMIP6 climate models (with AMOC index values ranging from 9.6 to 23.04 Sv; Weijer et al., 2020), both FIO–ESM v2.0 and v2.1 fit the observations relatively well. Fig. 10 also shows that the AMOC index simulated by FIO–ESM v2.1 is slightly larger than that simulated by v2.0. The mean AMOC index values over the last century from FIO–ESM v2.0 and v2.1 are 20.4 and 21.5 Sv, respectively, which may explain the higher North Atlantic Ocean SST in FIO–ESM v2.1 (Fig. 9f). A similar AMOC response to different ice–ocean heat exchange parameterizations in another climate model (COSMOS) was reported by Shi et al. (2021).

Arctic and Antarctic sea ice concentrations in March and September averaged over 1979–2014 simulated by FIO–ESM v2.0 and v2.1 are compared with satellite observations (EUMETSAT OSISAF, 2017). Winter differences (March in the Arctic, September in the Antarctic) in sea ice concentration between FIO–ESM v2.0 and v2.1 are comparatively small, as both models fit satellite observations well (Figs. 11a–c, 12d–f); however, summer differences (September in Arctic, and March in Antarctic) are notable. For the Arctic, the FIO–ESM v2.0 *Historical* experiment severely underestimates summer sea ice concentration (Fig. 11e), particularly in the Arctic marginal seas (including the East Siberian Sea, Laptev Sea, Kara Sea, and Beaufort Sea), where no regional sea ice is simulated during 1979–2014. These underestimation biases are significantly reduced in FIO–ESM v2.1 (Fig. 11f). For the Antarctic, the summer sea ice concentration is also underestimated by FIO–ESM v2.0 (Fig. 12b), and larger sea ice concentration is simulated by FIO–ESM v2.1 (Fig. 12c), but FIO-ESM v2.1 overestimates the sea ice

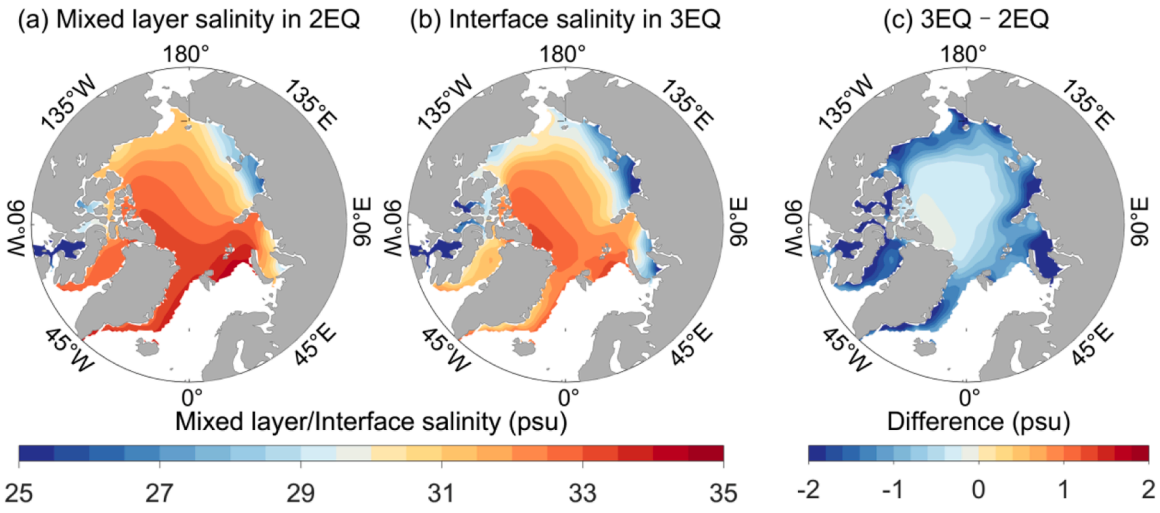

Fig. 3. Mixed layer salinity and ice–ocean interface salinity in August during 1950–1979 simulated by FIO–ESM v2.1 (a) *2EQ* and (b) *3EQ* experiments, and (c) the differences between the two numerical experiments. The sea ice component model used in the two experiments is CICE6.0.

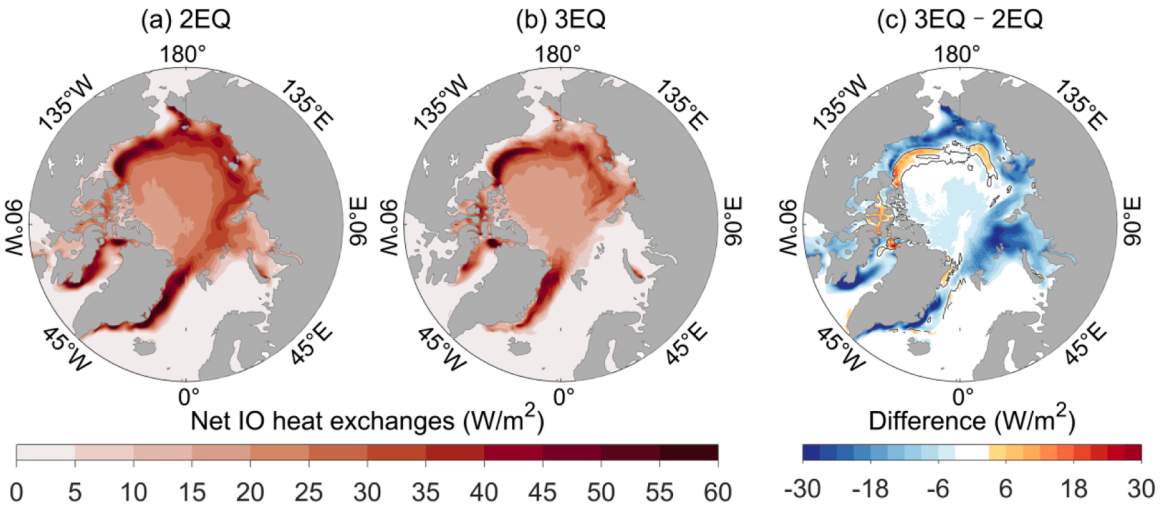

Fig. 4. August ice–ocean (IO) net heat exchanges over the Arctic Ocean during 1950–1979 simulated by FIO–ESM v2.1 (a) *2EQ* and (b) *3EQ* experiments, and (c) the differences between the two numerical experiments. The sea ice component model used in the two experiments is CICE6.0.

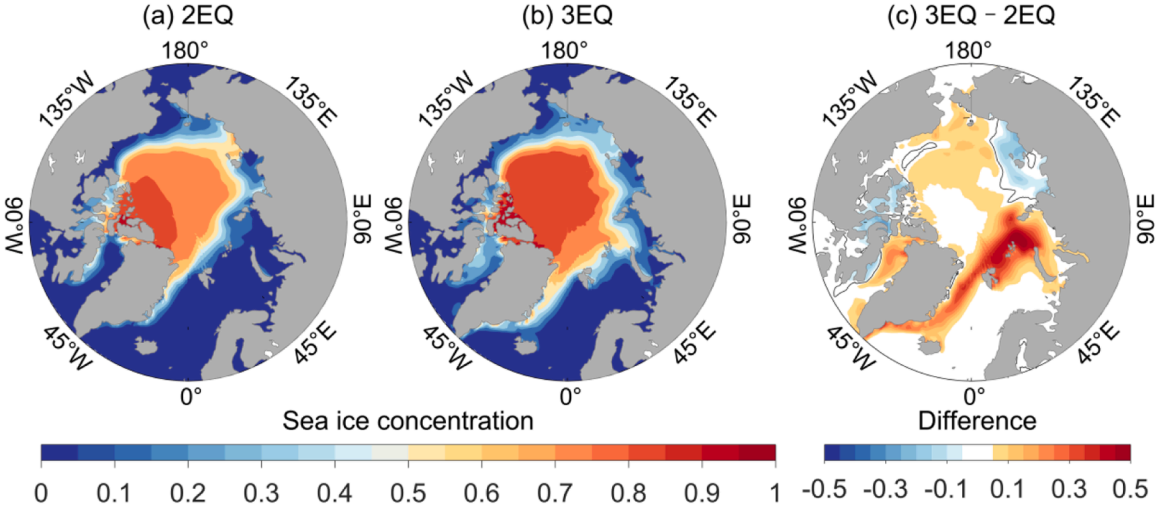

Fig. 5. August Arctic sea ice concentration during 1950–1979 simulated by FIO–ESM v2.1 (a) *2EQ* and (b) *3EQ* experiments, and (c) the differences between two numerical experiments. The sea ice component model used in the two experiments is CICE6.0.

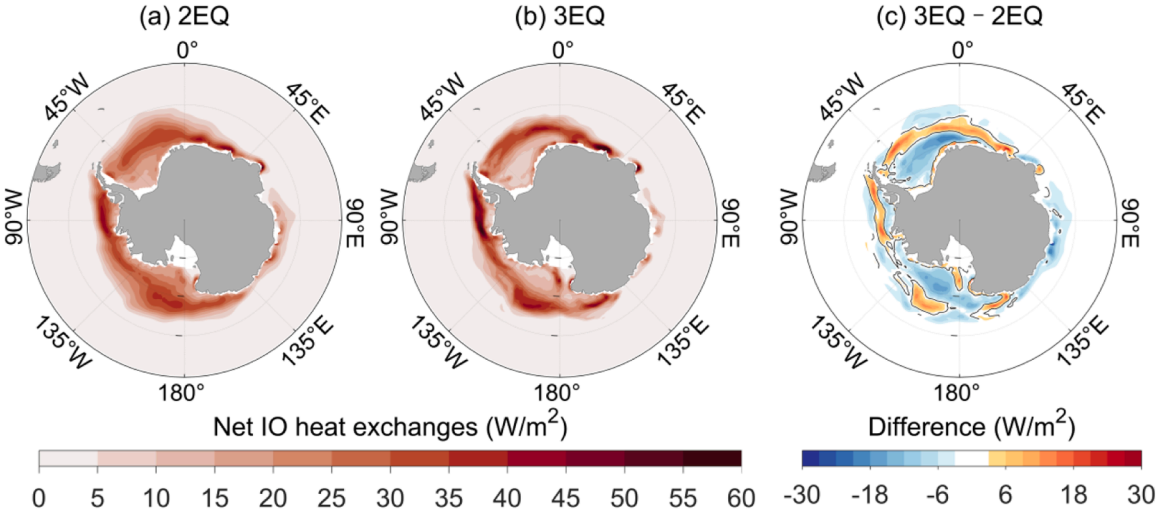

Fig. 6. February ice–ocean (IO) net heat exchanges in the Southern Ocean during 1950–1979 simulated by FIO–ESM v2.1 (a) *2EQ* and (b) *3EQ* experiments, and (c) the differences between the two numerical experiments. The sea ice component model used in the two experiments is CICE6.0.

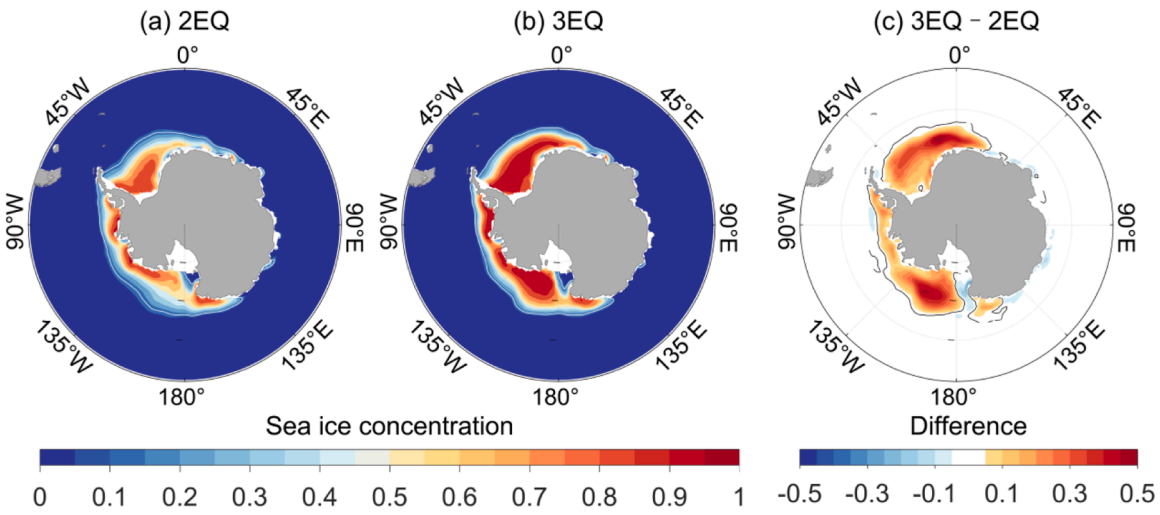

Fig. 7. February Antarctic sea ice concentration during 1950–1979 simulated by FIO–ESM v2.1 (a) *2EQ* and (b) *3EQ* experiments, and (c) the differences between the two numerical experiments. The sea ice component model used in the two experiments is CICE6.0.

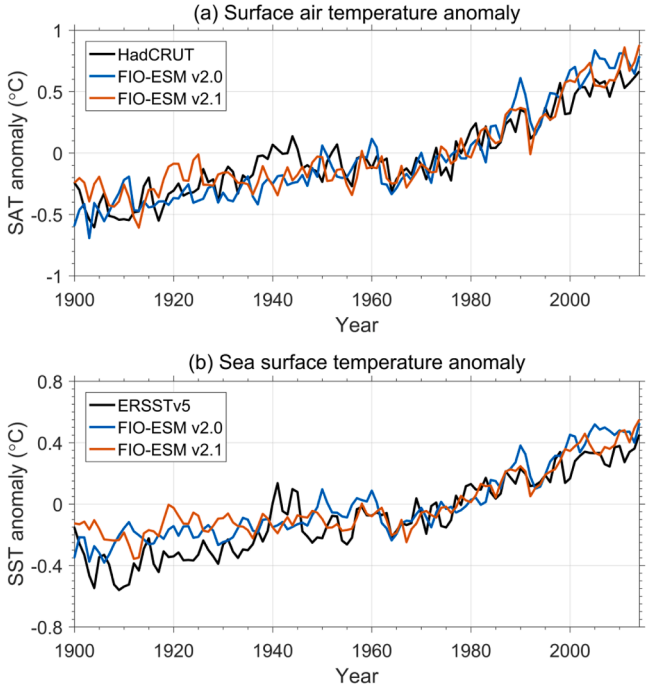

Fig. 8. Time series of annual–mean global averaged (a) surface air temperature (SAT) and (b) sea surface temperature (SST) anomalies from HadCRUT (Morice et al., 2021) and ERSST5 (Huang et al., 2017), respectively, as well as FIO–ESM v2.0 and FIO–ESM v2.1 *Historical* simulations. The anomalies are relative to 1961–1990.

concentration in the Weddell Sea, Bellingshausen Sea, and Ross Sea.

Fig. 13 shows the Arctic sea ice thickness in March during 2011–2014 from the merged CryoSat-2 and SMOS satellite data (Ricker et al., 2017) and simulations by FIO–ESM v2.0 and FIO–ESM v2.1. It indicates that both FIO–ESM v2.0 and FIO–ESM v2.1 can reproduce the spatial pattern of observed sea ice thickness. However, FIO–ESM v2.1 significantly overestimates it, especially in thick ice regions. The sea ice thickness is less than 3 m north of the Canadian Arctic Archipelago and Greenland based on satellite observations, but it is greater than 5 m in FIO–ESM v2.1. Sea ice thickness simulations by FIO–ESM v2.1 should be further improved in the future.

3.4. Arctic and Antarctic sea ice extent projections under FIO–ESM v2.1

The projection of future Arctic sea ice changes draws substantial attention for its significant potential impacts on regional maritime activities and marine ecosystems, in addition to weather and climate systems at mid– and high–latitudes (Lannuzel et al., 2020; Min et al., 2022; Mori et al., 2014; Sévellec et al., 2017). Previous studies have shown that projected future changes in Arctic sea ice by climate models are highly dependent upon their simulation conditions during historical periods (Hall et al., 2019; Liu et al., 2013; Wang et al., 2021). Here, both the climatological state and long–term trends of Arctic SIE during 1979–2014 simulated by FIO–ESM v2.1 fit the satellite observations well (Fig. 14a, b). It projects that winter Arctic sea ice will continue to decline in a warming climate under all three scenarios, and an abrupt loss of winter SIE is projected to occur in the 2080s under SSP5–8.5. Several CMIP5 climate models also project a similar abrupt ice loss in the Arctic (Hankel and Tziperman, 2021), but the emergence time projected by CMIP5 models is later (after 2100). Similarly, FIO–ESM v2.1 projected that summer Arctic sea ice will continue to decline rapidly under all three scenarios (Fig. 14b). Even under SSP1–2.6, the September Arctic SIE will fall below the ice–free threshold (1.0 million km^2) before 2100. Under SSP2–4.5 and SSP5–8.5, the first ice-free Arctic projected by FIO–ESM v2.1 will occur in the 2050s and 2040s, respectively. This is earlier than the CMIP6 multi–model mean (MMM) results, which indicate a likely ice–free Arctic September by 2076 and 2055 under the same two scenarios, respectively (Wei et al., 2020). It should be mentioned that the FIO–ESM v2.1 projections more closely align with observationally constrained projections that predict an ice–free Arctic summer near 2035 (Docquier and Koenigk, 2021).

FIO–ESM v2.1 also projects further declining Antarctic sea ice in a warming climate (Fig. 14c, d). When the same threshold (1.0 million km^2) is applied to the Antarctic, the first ice–free Antarctic summers are projected to occur in the 2070s and 2050s under scenarios SSP2–4.5 and SSP5–8.5, respectively; however, similar to most CMIP5 and CMIP6 climate models, FIO–ESM v2.1 is unable to successfully reproduce the observed increase in SIE across the Antarctic during the satellite period (Shu et al., 2020, 2015). This discrepancy between simulations and satellite observations of Antarctic SIE is likely caused by model biases and considerable interannual sea ice variability (Polvani and Smith, 2013; Shu et al., 2020; Sun and Eisenman, 2021; Zunz et al., 2013). The observed positive trend of Antarctic SIE can be reproduced by climate models by removing the biases of the simulated sea ice drift velocity (Sun and Eisenman, 2021).

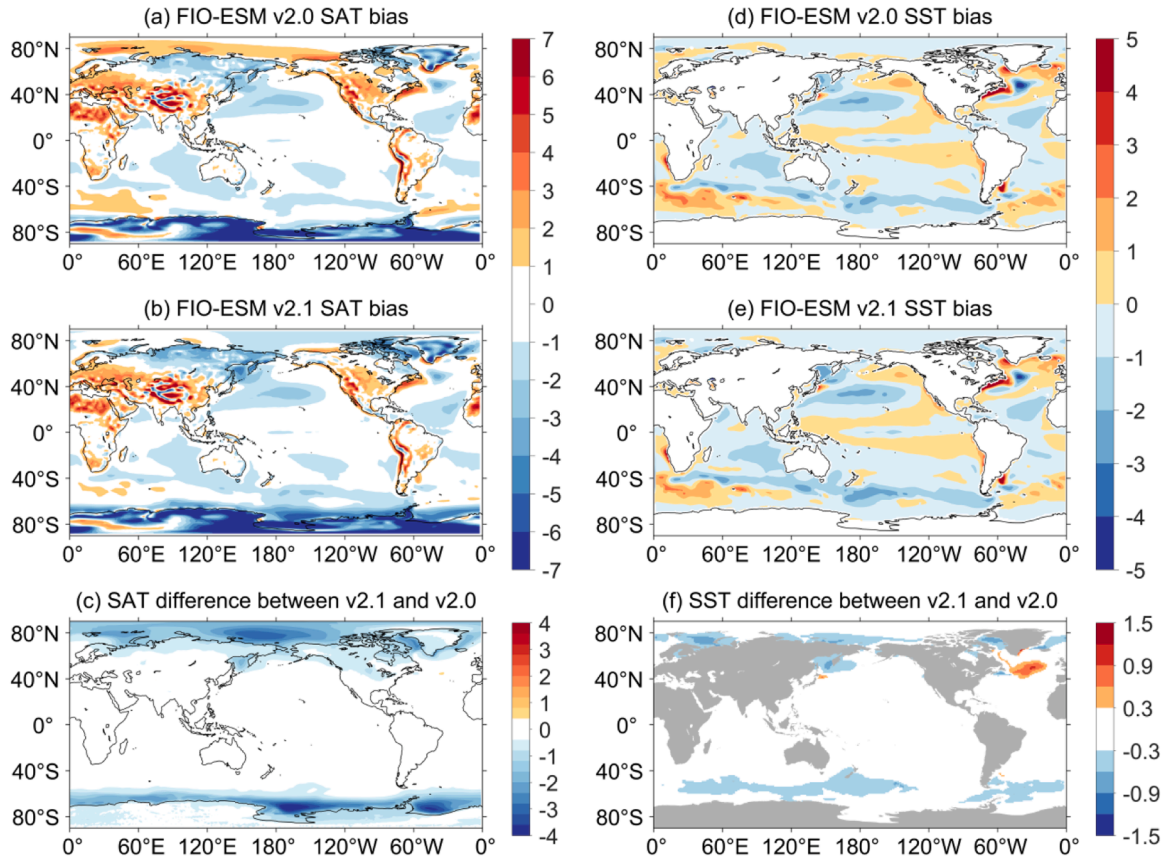

Fig. 9. Annual-mean SAT and SST biases, along with the differences between FIO–ESM v2.1 and FIO–ESM v2.0 *Historical* experiments. Biases of SAT are calculated as the differences between simulations and NCEP–DOE reanalysis 2 (Kanamitsu et al., 2002); whereas biases of SST are derived as the differences between simulations and WOA18 (Locarnini et al., 2018). The time periods of the SAT and SST analyses are 1979–2014 and 1975–2004, respectively.

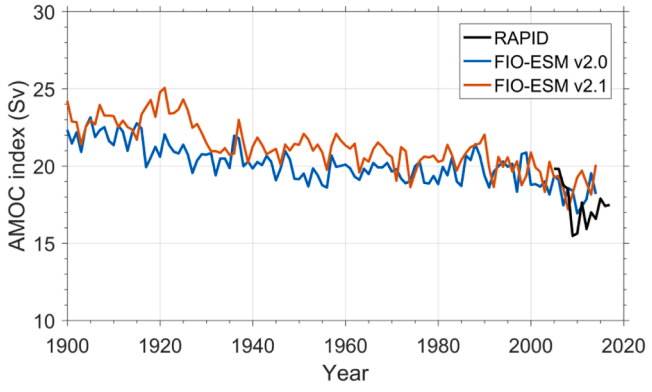

Fig. 10. Time series of AMOC index values from RAPID/MOCHA observations (Moat et al., 2022) against the FIO–ESM v2.0 and FIO–ESM v2.1 *Historical* simulations.

4. Discussion and conclusions

In this study, the latest version of FIO–ESM (v2.1) has been developed, and its performances are evaluated via comparisons with observations and FIO–ESM v2.0 simulations. Specifically, the sea ice component model of FIO–ESM v2.1 is updated from CICE4.0 of v2.0 to CICE6.0, while the ice–ocean heat exchange parameterization is improved from a 2EQ to a more realistic 3EQ boundary condition parameterization. Numerical experiments show that FIO–ESM v2.1 performs well during simulations of Arctic SIE, SAT, SST, and AMOC. The influences of version updating are mainly at high latitudes. The biases of the underestimation of Arctic summer SIE in FIO–ESM v2.0 have been significantly reduced by the updating of the sea ice component model and the improvement of the ice-ocean heat exchange parameterization. Accordingly, both the climatology and long–term trends of Arctic SIE during the satellite era are well reproduced with FIO–ESM v2.1. However, summer Antarctic SIE is overestimated with larger biases in FIO–ESM v2.1 compared to FIO–ESM v2.0.

Furthermore, the analysis results here show that under the framework of FIO–ESM, CICE6.0 simulates more summer sea ice than CICE4.0 across both the Arctic and Antarctic regions, notably similar to previous Arctic results based on standalone sea ice model simulations (Wang et al., 2020). Compared with the ice–ocean heat flux 2EQ parameterization, the 3EQ parameterization reduces ice–ocean net heat exchange during the melt season, and causes higher sea ice concentration and SIE in the Arctic summer (also similar to previous standalone sea ice model results; Yu et al., 2022). As a result, advancing from 2EQ to 3EQ parameterization can reduce the underestimation of Arctic summer SIE in fully coupled climate models. The influences of 3EQ parameterization on Antarctic SIE are insignificant, although its impacts on Antarctic ice–ocean net heat exchange and sea ice concentration are notable.

Although the climatology of sea ice extent simulations is improved by new sea ice physical processes from FIO–ESM v2.0 to FIO–ESM v2.1, the sensitivity of sea ice extent to global warming is not affected by these processes. Fig. 15 shows that the relationships between the changes of Arctic sea ice extent and global–mean SAT in FIO–ESM v2.0 and FIO–ESM v2.1 are nearly the same. It indicates that the sensitivity of sea ice extent to global warming is a similar constant scaling factor in FIO–ESM v2.0 and FIO–ESM v2.1, so the simulated Arctic sea ice sensitivity is not significantly affected by the new sea ice physical processes. This is consistent with previous studies (Rosenblum and Eisenman, 2017, 2016;

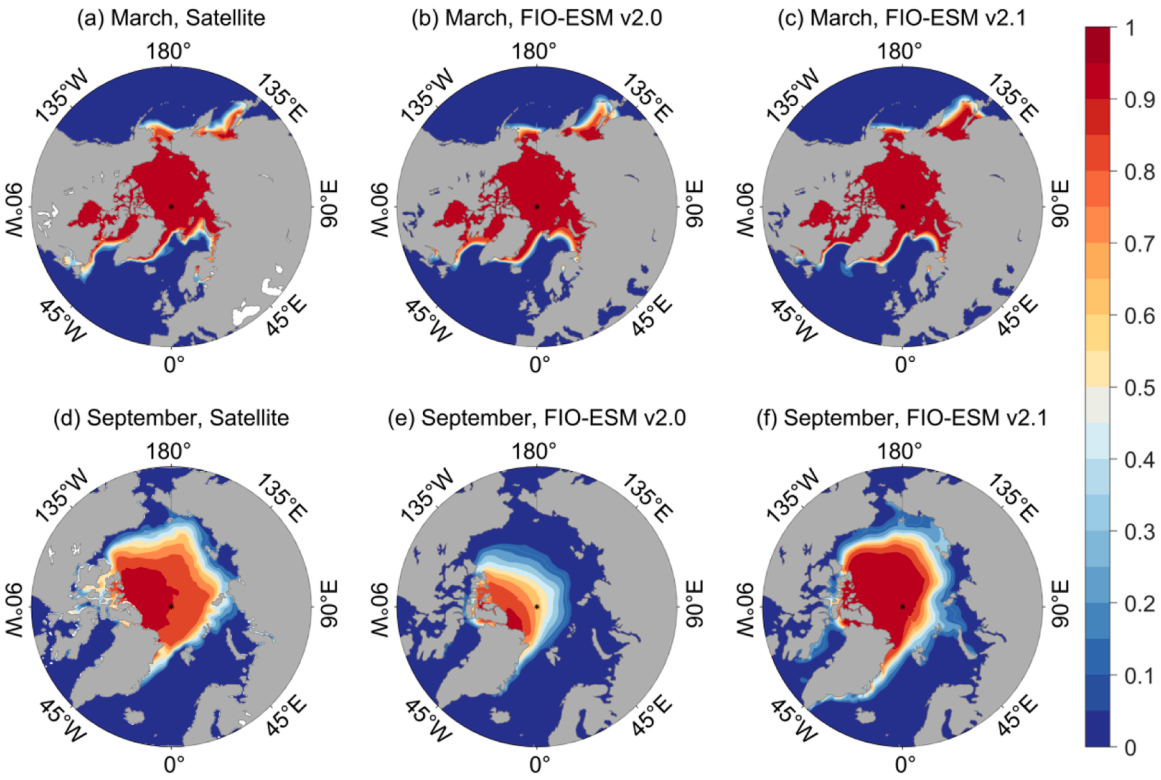

Fig. 11. Arctic sea ice concentration in March and September during 1979–2014 based on satellite observations (EUMETSAT OSISAF, 2017) and *Historical* simulations by FIO–ESM v2.0 and FIO–ESM v2.1.

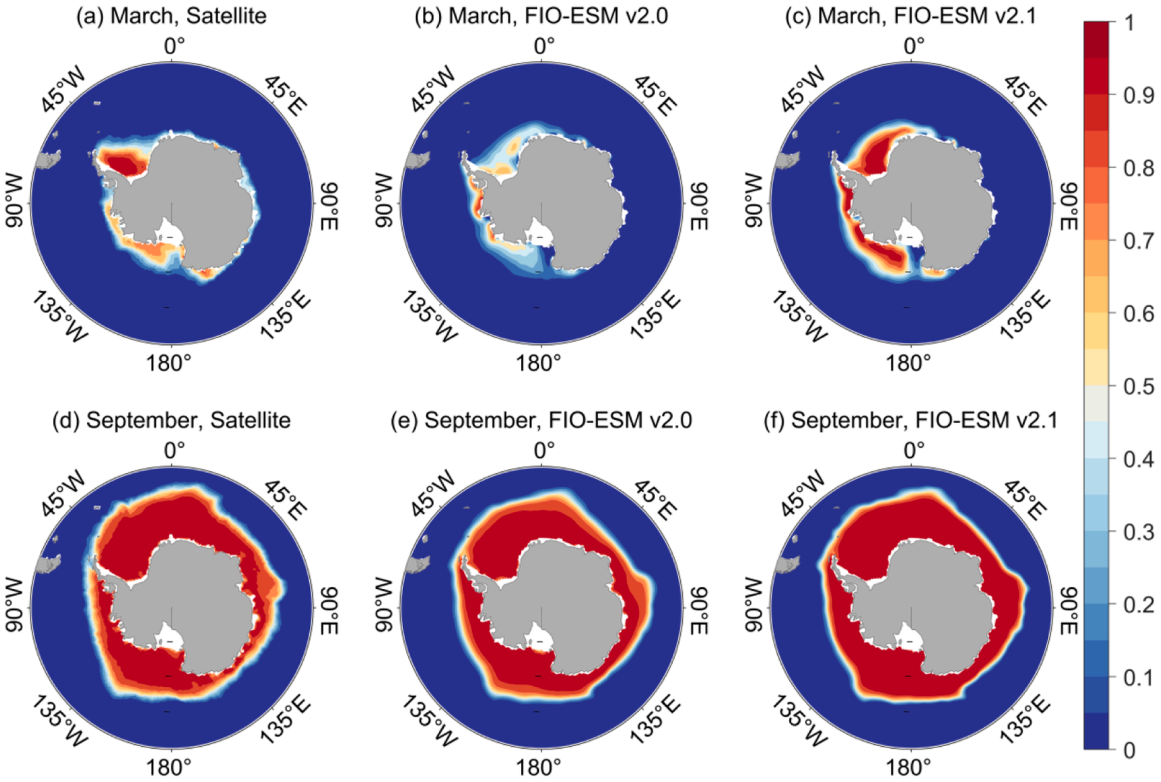

Fig. 12. Antarctic sea ice concentration in March and September during 1979–2014 based on satellite observations (EUMETSAT OSISAF, 2017) and *Historical* simulations by FIO–ESM v2.0 and FIO–ESM v2.1.

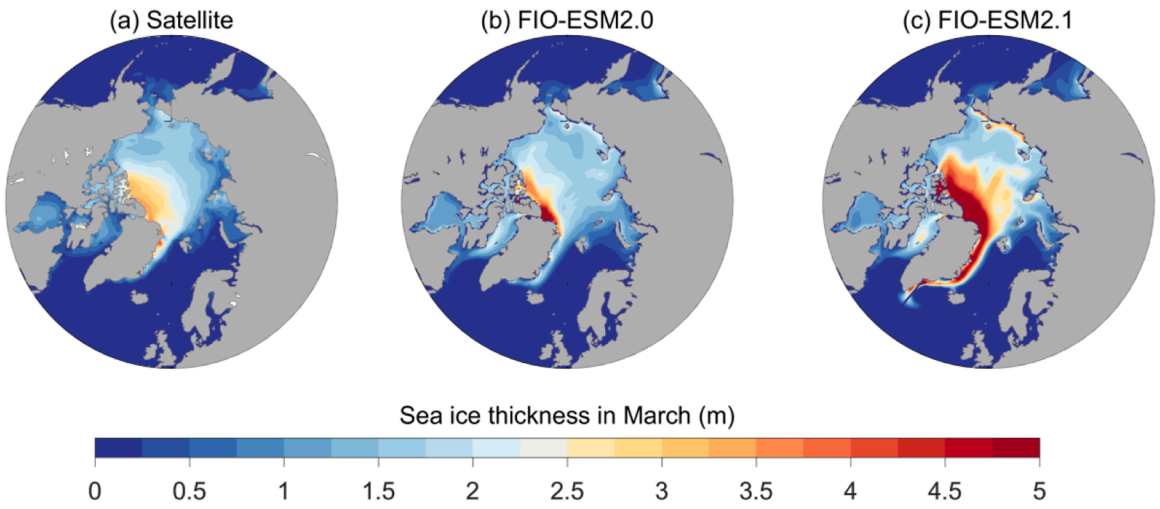

Fig. 13. March sea ice thickness in the Arctic during 2011–2014 based on satellite observations (Ricker et al., 2017) and *Historical* simulations by FIO–ESM v2.0 and FIO–ESM v2.1.

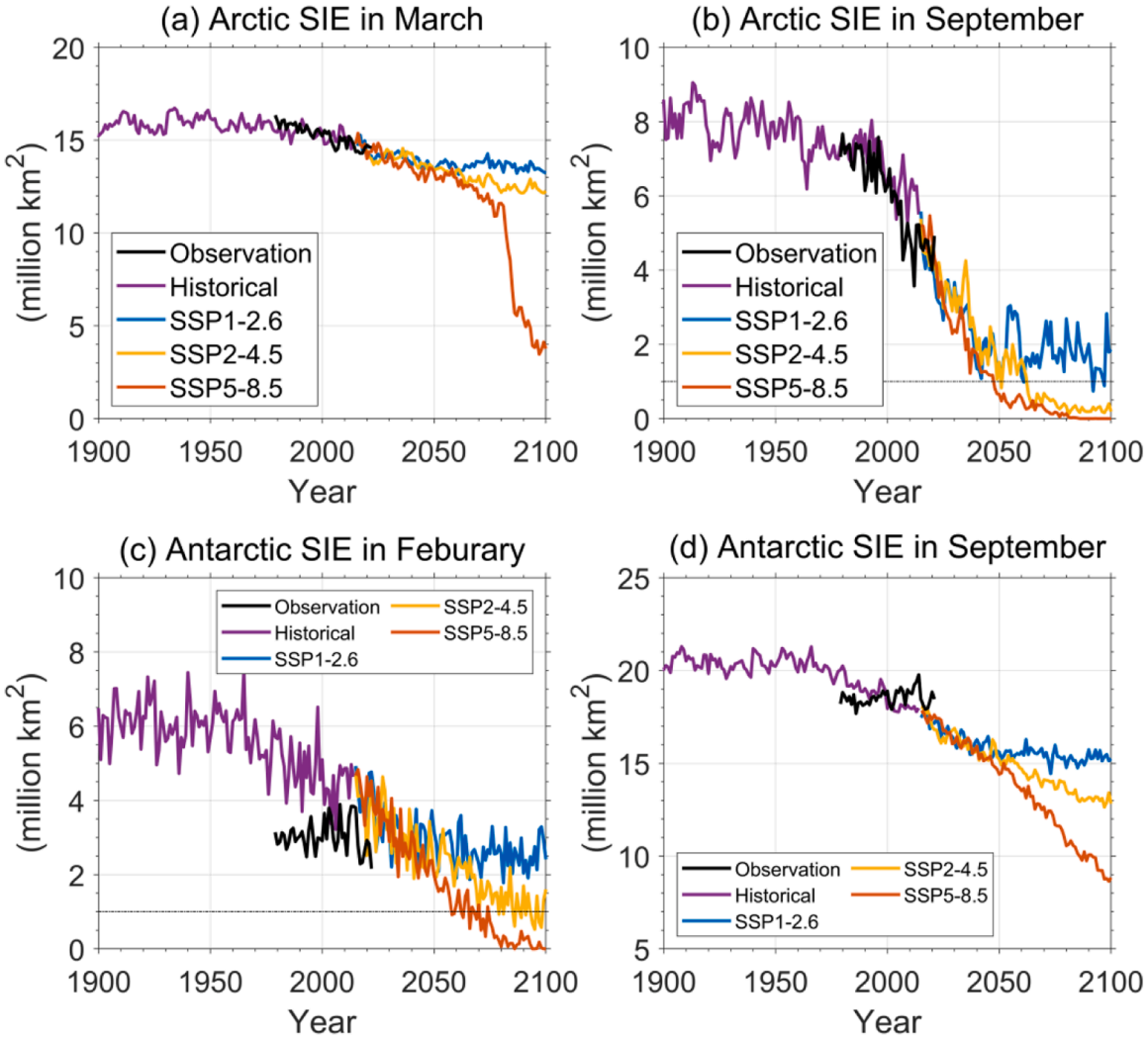

Fig. 14. Arctic and Antarctic sea ice extent (SIE) in February/March and September based on FIO–ESM v2.1 *Historical* and *SSP(1-2.6, 2-4.5*, and *5-8.5)* simulations. Back lines are the satellite observations (Fetterer et al., 2017). Black dashed lines in (b) and (c) represent the ice–free threshold (1.0 million km^2).

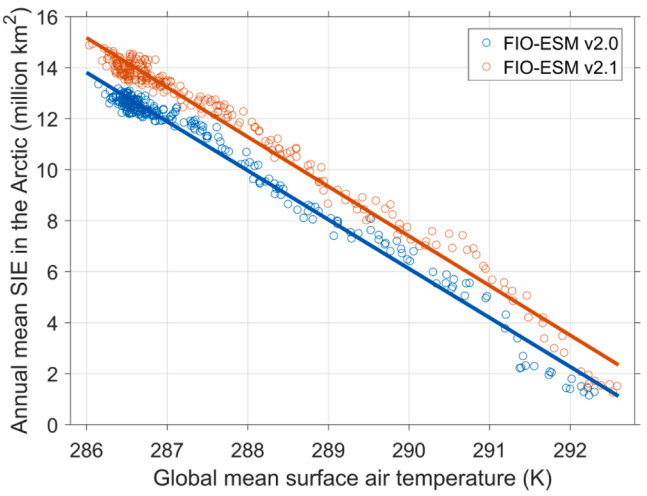

Fig. 15. Global mean surface air temperature and annual mean sea ice extent (SIE) in the Arctic for FIO–ESM v2.0 and FIO–ESM v2.1 *Historical and SSP5-8.5* simulations.

Winton, 2011).

Arctic sea ice decline has potential effects on regional marine ecosystems, as well as the global climate system and human activities. Furthermore, Arctic sea ice projections under FIO–ESM v2.1 are also investigated in this study. The results show that the first ice–free Arctic summer will occur in the 2050s and 2040s under scenarios SSP2–4.5 and SSP5–8.5, respectively. FIO–ESM v2.1 also projects an abrupt Arctic winter sea ice loss event in the 2080s under SSP5–8.5, markedly earlier than projections based on CMIP5 (Hankel and Tziperman, 2021).

Although CICE6.0 includes more physical processes than CICE4.0, the biases of Antarctic summer SIE become larger after version updating from FIO–ESM v2.0 to v2.1. Some model parameters are set to different default values in CICE4.0 and CICE6.0. Many parameters in the sea ice model were mainly determined based on observations in the Arctic but not the Antarctic. Therefore, this may cause smaller sea ice biases in the Arctic but larger biases in the Antarctic. Sea ice biases may have also arisen from other component models, such as the incorporated atmospheric and/or ocean models. Further studies are still needed to improve Antarctic sea ice simulations by FIO–ESM.

CRediT authorship contribution statement

Qi Shu: Writing – original draft, Methodology, Software, Visualization. **Fangli Qiao:** Conceptualization, Supervision, Writing – review & editing. **Jiping Liu:** Methodology, Writing – review & editing, Validation. **Ying Bao:** Data curation, Investigation, Writing – review & editing. **Zhenya Song:** Conceptualization, Funding acquisition, Resources, Project administration, Writing – review & editing, Visualization.

Declaration of Competing Interest

The authors declare that they have no known competing financial interests or personal relationships that could have appeared to influence the work reported in this paper.

Data availability

Data will be made available on request.

Acknowledgments

We would like to thank Prof. Ian Eisenman and the other anonymous reviewer for their helpful comments and suggestions that improved this manuscript. We thank Dr. Xiaoxu Shi for useful discussions. This work was supported by the Basic Scientific Fund for National Public Research Institute of China (2023S01), National Natural Science Foundation of China (42276253, 42022042, and 41821004), Shandong Provincial Natural Science Foundation (ZR2022JQ17), the Taishan Scholar Foundation of Shandong Province (tsqn202211264), and China–Korea Cooperation Project on Northwest Pacific Marine Ecosystem Simulation under Climate Change.

References

Bao, Y., Song, Z., Qiao, F., 2020. FIO–ESM version 2.0: Model description and evaluation. J. Geophys. Res. Ocean 125 (6), e2019JC016036. https://doi.org/10.1029/2019JC016036.

Bitz, C.M., Lipscomb, W.H., 1999. An energy–conserving thermodynamic model of sea ice. J. Geophys. Res. Ocean. 104 (C7), 15669–15677. https://doi.org/10.1029/1999JC900100.

Docquier, D., Koenigk, T., 2021. Observation–based selection of climate models projects Arctic ice–free summers around 2035. Commun. Earth Environ. 2, 114. https://doi.org/10.1038/s43247–021–00214–7.

Duvivier A., 2018. CICE–consortium documentation. https://buildmedia.readthedocs.org/media/pdf/cicea/latest/cicea.pdf. Date Accessed 07–30–2023.

EUMETSAT Ocean and Sea Ice Satellite Application Facility (OSISAF), 2017. Global sea ice concentration climate data record 1979-2015 (v2.0), OSI-450. doi: 10.15770/EUM_SAF_OSI_0008. Date Accessed 07–30–2023.

Eyring, V., Bony, S., Meehl, G.A., Senior, C.A., Stevens, B., Stouffer, R.J., Taylor, K.E., 2016. Overview of the coupled model intercomparison project phase 6 (CMIP6) experimental design and organization. Geosci. Model Dev. 9 (5), 1937–1958. https://doi.org/10.5194/gmd–9–1937–2016.

Fetterer F., Knowles K., Meier W.N., Savoie M., Windnagel A.K., 2017. Sea ice index, version 3: sea ice extent. boulder, CO USA. National Snow and Ice Data Center. 10.7265/N5K072F8. Date Accessed 07–30–2023.

Griffies, S.M., Biastoch, A., Böning, C., Bryan, F., Danabasoglu, G., Chassignet, E.P., England, M.H., Gerdes, R., Haak, H., Hallberg, R.W., Hazeleger, W., Jungclaus, J., Large, W.G., Madec, G., Pirani, A., Samuels, B.L., Scheinert, M., Gupta, A.S, Severijns, C.A., Simmons, H.L., Treguier, A.M., Winton, M., Yeager, S., Yin, J., 2009. Coordinated ocean-ice reference experiments (COREs). Ocean Model 26, 1–46. https://doi.org/10.1016/j.ocemod.2008.08.007.

Griffies, S.M., Danabasoglu, G., Durack, P.J., Adcroft, A.J., Balaji, V., Böning, C.W., Chassignet, E.P., Curchitser, E., Deshayes, J., Drange, H., Fox-Kemper, B., Gleckler, P.J., Gregory, J.M., Haak, H., Hallberg, R.W., Heimbach, P., Hewitt, H.T., Holland, D.M., Ilyina, T., Jungclaus, J.H., Komuro, Y., Krasting, J.P., Large, W.G., Marsland, S.J., Masina, S., McDougall, T.J., George Nurser, A.J., Orr, J.C., Pirani, A., Qiao, F., Stouffer, R.J., Taylor, K.E., Treguier, A.M., Tsujino, H., Uotila, P., Valdivieso, M., Wang, Q., Winton, M., Yeager, S.G., 2016. OMIP contribution to CMIP6: experimental and diagnostic protocol for the physical component of the ocean model intercomparison project. Geosci. Model Dev. 9, 3231–3296. https://doi.org/10.5194/gmd-9-3231-2016.

Hall, A., Cox, P., Huntingford, C., Klein, S., 2019. Progressing emergent constraints on future climate change. Nat. Clim. Chang. 9, 269–278. https://doi.org/10.1038/s41558–019–0436–6.

Hankel, C., Tziperman, E., 2021. The role of atmospheric feedbacks in abrupt winter Arctic sea ice loss in future warming scenarios. J. Clim. 34 (11), 4435–4447. https://doi.org/10.1175/JCLI–D–20–0558.1.

Huang, B., Thorne, P.W., Banzon, V.F., Boyer, T., Chepurin, G., Lawrimore, J.H., Menne, M.J., Smith, T.M., Vose, R.S., Zhang, H.M., 2017. Extended reconstructed sea surface temperature, version 5 (ERSSTv5): upgrades, validations, and intercomparisons. J. Clim. 30 (20), 8179–8205. https://doi.org/10.1175/JCLI–D–16–0836.1.

Hunke, E., Lipscomb, W., 2010. CICE: The Los Alamos Sea Ice Model Documentation and Software User's Manual Version 4.0. Tech. Rep. LA–CC–06–012. Los Alamos National Laboratory, Los Alamos, NM USA.

Intergovernmental Panel on Climate Change (IPCC), 2014. Evaluation of climate models. Climate Change 2013 – The Physical Science Basis. Cambridge University Press, Cambridge, pp. 741–866. https://doi.org/10.1017/CBO9781107415324.020. Working Group I Contribution to the Fifth Assessment Report of the Intergovernmental Panel on Climate Change.

Kanamitsu, M., Ebisuzaki, W., Woollen, J., Yang, S., Hnilo, J.J., Fiorino, M., Potter, G.L., 2002. NCEP–DOE AMIP–II reanalysis (R–2). Bull. Am. Meteorol. Soc. 83 (11), 1631–1644. https://doi.org/10.1175/BAMS–83–11–1631.

Lannuzel, D., Tedesco, L., van Leeuwe, M., Campbell, K., Flores, H., Delille, B., Miller, L., Stefels, J., Assmy, P., Bowman, J., Brown, K., Castellani, G., Chierici, M., Crabeck, O., Damm, E., Else, B., Fransson, A., Fripiat, F., Geilfus, N.X., Jacques, C., Jones, E., Kaartokallio, H., Kotovitch, M., Meiners, K., Moreau, S., Nomura, D., Peeken, I., Rintala, J.M., Steiner, N., Tison, J.L., Vancoppenolle, M., Van der Linden, F., Vichi, M., Wongpan, P., 2020. The future of Arctic sea–ice biogeochemistry and ice–associated ecosystems. Nat. Clim. Chang. 10, 983–992. https://doi.org/10.1038/s41558–020–00940–4.

Lawrence, D.M., Oleson, K.W., Flanner, M.G., Thornton, P.E., Swenson, S.C., Lawrence, P.J., Zeng, X., Yang, Z.L., Levis, S., Sakaguchi, K., Bonan, G.B., Slater, A. G., 2011. Parameterization improvements and functional and structural advances in

version 4 of the community land model. J. Adv. Model. Earth Syst. 3 (1), M03001. https://doi.org/10.1029/2011MS00045.
Lee, J., Planton, Y.Y., Gleckler, P.J., Sperber, K.R., Guilyardi, E., Wittenberg, A.T., McPhaden, M.J., Pallotta, G., 2021. Robust Evaluation of ENSO in climate models: How many ensemble members are needed? Geophys. Res. Lett. 48 (20), e2021GL095041 https://doi.org/10.1029/2021GL095041.
Liu, J., Song, M., Horton, R.M., Hu, Y., 2013. Reducing spread in climate model projections of a September ice–free Arctic. Proc. Natl. Acad. Sci. U. S. A. 110 (31), 12571–12576. https://doi.org/10.1073/pnas.1219716110.
Locarnini, R.A., Mishonov, A.V, Baranova, O.K., Boyer, T.P., Zweng, M.M., Garcia, H.E., Reagan, J.R., Seidov, D., Weathers, K.W., Paver, C.R., Smolyar, I.V, 2019. World Ocean Atlas 2018, 1. Temperature. NOAA Atlas NESDIS 81, p. 52.
Min, C., Yang, Q., Chen, D., Yang, Y., Zhou, X., Shu, Q., Liu, J., 2022. The emerging Arctic shipping corridors. Geophys. Res. Lett. 49 (10), e2022GL099157 https://doi.org/10.1029/2022GL099157.
Moat, B.I., Frajka-Williams, E., Smeed, D.A., Rayner, D., Johns, W.E., Baringer, M.O., Volkov, D., Collins, J., 2022. Atlantic meridional overturning circulation observed by the RAPID-MOCHA-WBTS (RAPID-Meridional Overturning Circulation and Heatflux Array-Western Boundary Time Series) array at 26N from 2004 to 2020 (v2020.2), British Oceanographic Data Centre. Natural Environment Research Council, UK. https://doi.org/10.5285/e91b10af-6f0a-7fa7-e053-6c86abc05a09. Accessed 07–30–2023.
Mori, M., Watanabe, M., Shiogama, H., Inoue, J., Kimoto, M., 2014. Robust Arctic sea–ice influence on the frequent Eurasian cold winters in past decades. Nat. Geosci. 7, 869–873. https://doi.org/10.1038/ngeo2277.
Morice, C.P., Kennedy, J.J., Rayner, N.A., Winn, J.P., Hogan, E., Killick, R.E., Dunn, R.J. H., Osborn, T.J., Jones, P.D., Simpson, I.R., 2021. An updated assessment of near-surface temperature change from 1850: The HadCRUT5 data set. J. Geophys. Res. Atmos. 126 (3), e2019JD032361 https://doi.org/10.1029/2019JD032361.
Neale, R.B., Gettelman, A., Park, S., Chen, C., Lauritzen, P.H., Williamson, D.L., Conley, A.J., Kinnison, D., Marsh, D., Smith, A.K., Vitt, F., Garcia, R., Lamarque, J., Mills, M., Tilmes, S., Morrison, H., Cameron–smith, P., Collins, W.D., Iacono, M.J., Easter, R.C., Liu, X., Ghan, S.J., Rasch, P.J., Taylor, M.A, 2012. Description of the NCAR community atmosphere model (CAM 5.0) (NCAR/TN–486+STR). https://doi.org/10.5065/wgtk–4g06.
O'Neill, B.C., Tebaldi, C., Van Vuuren, D.P., Eyring, V., Friedlingstein, P., Hurtt, G., Knutti, R., Kriegler, E., Lamarque, J.F., Lowe, J., Meehl, G.A., Moss, R., Riahi, K., Sanderson, B.M., 2016. The scenario model intercomparison project (ScenarioMIP) for CMIP6. Geosci. Model Dev. 9 (9), 3461–3482. https://doi.org/10.5194/gmd–9–3461–2016.
Onarheim, I.H., Eldevik, T., Smedsrud, L.H., Stroeve, J.C., 2018. Seasonal and regional manifestation of Arctic sea ice loss. J. Clim. 31 (12), 4917–4932. https://doi.org/10.1175/JCLI–D–17–0427.1.
Polvani, L.M., Smith, K.L., 2013. Can natural variability explain observed Antarctic sea ice trends? New modeling evidence from CMIP5. Geophys. Res. Lett 40 (12), 3195–3199. https://doi.org/10.1002/grl.50578.
Qiao, F., Song, Z., Bao, Y., Song, Y., Shu, Q., Huang, C., Zhao, W., 2013. Development and evaluation of an Earth system model with surface gravity waves. J. Geophys. Res. Ocean 118 (9), 4514–4524. https://doi.org/10.1002/jgrc.20327.
Qiao, F., Yuan, Y., Yang, Y., Zheng, Q., Xia, C., Ma, J., 2004. Wave–induced mixing in the upper ocean: distribution and application to a global ocean circulation model. Geophys. Res. Lett. 31 (11), L11303. https://doi.org/10.1029/2004GL019824.
Qiao, F., Zhao, W., Yin, X., Huang, X., Liu, X., Shu, Q., Wang, G., Song, Z., Li, X., Liu, H., 2016. A highly effective global surface wave numerical simulation with ultra–high resolution. In: SC'16: Proceedings of the International Conference for High Performance Computing, Networking, Storage and Analysis. IEEE, pp. 46–56. https://doi.org/10.1109/SC.2016.4.
Riahi, K., van Vuuren, D.P., Kriegler, E., Edmonds, J., O'Neill, B.C., Fujimori, S., Bauer, N., Calvin, K., Dellink, R., Fricko, O., Lutz, W., Popp, A., Cuaresma, J.C., KC, S., Leimbach, M., Jiang, L., Kram, T., Rao, S., Emmerling, J., Ebi, K., Hasegawa, T., Havlik, P., Humpenöder, F., Da Silva, L.A., Smith, S., Stehfest, E., Bosetti, V., Eom, J., Gernaat, D., Masui, T., Rogelj, J., Strefler, J., Drouet, L., Krey, V., Luderer, G., Harmsen, M., Takahashi, K., Baumstark, L., Doelman, J.C., Kainuma, M., Klimont, Z., Marangoni, G., Lotze–Campen, H., Obersteiner, M., Tabeau, A., Tavoni, M., 2017. The Shared Socioeconomic Pathways and their energy, land use, and greenhouse gas emissions implications: an overview. Glob. Environ. Chang. 42, 153–168. https://doi.org/10.1016/j.gloenvcha.2016.05.009.
Ricker, R., Hendricks, S., Kaleschke, L., Tian-Kunze, X., King, J., Haas, C., 2017. A weekly Arctic sea-ice thickness data record from merged CryoSat-2 and SMOS satellite data. Cryosphere 11, 1607–1623. https://doi.org/10.5194/tc-11-1607-2017.
Rosenblum, E., Eisenman, I., 2017. Sea ice trends in climate models only accurate in runs with biased global warming. J. Clim. 30, 6265–6278. https://doi.org/10.1175/JCLI-D-16-0455.1.
Rosenblum, E., Eisenman, I., 2016. Faster Arctic sea ice retreat in CMIP5 than in CMIP3 due to volcanoes. J. Clim. 29, 9179–9188. https://doi.org/10.1175/JCLI-D-16-0391.1.
Sévellec, F., Fedorov, A.V., Liu, W., 2017. Arctic sea–ice decline weakens the Atlantic meridional overturning circulation. Nat. Clim. Chang. 7, 604–610. https://doi.org/10.1038/NCLIMATE3353.
Shi, X., Notz, D., Liu, J., Yang, H., Lohmann, G., 2021. Sensitivity of Northern Hemisphere climate to ice–ocean interface heat flux parameterizations. Geosci. Model Dev. 14 (8), 4891–4908. https://doi.org/10.5194/gmd–14–4891–2021.
Shu, Q., Song, Z., Bao, Y., Yang, X., Song, Y., Li, X., Wei, M., Qiao, F., 2022. FIO–ESM v2.0 CORE2–forced experiment for the CMIP6 ocean Model Intercomparison Project. Acta Oceanol. Sin. 41, 22–31. https://doi.org/10.1007/s13131–022–2000–x.
Shu, Q., Song, Z., Qiao, F., 2015. Assessment of sea ice simulations in the CMIP5 models. Cryosphere 9 (1), 399–409. https://doi.org/10.5194/tc–9–399–2015.
Shu, Q., Wang, Q., Song, Z., Qiao, F., Zhao, J., Chu, M., Li, X., 2020. Assessment of sea ice extent in CMIP6 with comparison to observations and CMIP5. Geophys. Res. Lett. 47 (9), e2020GL087965 https://doi.org/10.1029/2020GL087965.
Smith R., Jones P., Briegleb B., Bryan F., Danabasoglu G., Dennis J., Dukowicz J., Eden C., Fox–Kemper B., Gent P., Hecht M., Jayne S., Jochum M., Large W., Lindsay K., Maltrud M., Norton N., Peacock S., Vertenstein M., Yeager S., 2010. The parallel ocean program (POP) reference manual: ocean component of the community climate system model (CCSM). Rep. LAUR–01853 141. http://n2t.net/ark:/85065/d70g3j4h.
Song, Y., Qiao, F., Liu, J., Shu, Q., Bao, Y., Wei, M., Song, Z., 2022. Effects of sea spray on large–scale climatic features over the Southern Ocean. J. Clim. 35 (14), 4645–4663. https://doi.org/10.1175/JCLI–D–21–0608.1.
Song, Z., Bao, Y., Zhang, D., Shu, Q., Song, Y., Qiao, F., 2020. Centuries of monthly and 3–hourly global ocean wave data for past, present, and future climate research. Sci. Data 7, 226. https://doi.org/10.1038/s41597–020–0566–8.
Stroeve, J., Notz, D., 2018. Changing state of Arctic sea ice across all seasons. Environ. Res. Lett. 13 (10), 103001 https://doi.org/10.1088/1748–9326/aade56.
Sun, S., Eisenman, I., 2021. Observed Antarctic sea ice expansion reproduced in a climate model after correcting biases in sea ice drift velocity. Nat. Commun. 12, 2–7. https://doi.org/10.1038/s41467-021-21412-z.
Tebaldi, C., Debeire, K., Eyring, V., Fischer, E., Fyfe, J., Friedlingstein, P., Knutti, R., Lowe, J., O'Neill, B., Sanderson, B., Van Vuuren, D., Riahi, K., Meinshausen, M., Nicholls, Z., Tokarska, K., Hurtt, G., Kriegler, E., Meehl, G., Moss, R., Bauer, S., Boucher, O., Brovkin, V., Yhb, Y., Dix, M., Gualdi, S., Guo, H., John, J., Kharin, S., Kim, Y.H., Koshiro, T., Ma, L., Olivié, D., Panickal, S., Qiao, F., Rong, X., Rosenbloom, N., Schupfner, M., Séférian, R., Sellar, A., Semmler, T., Shi, X., Song, Z., Steger, C., Stouffer, R., Swart, N., Tachiiri, K., Tang, Q., Tatebe, H., Voldoire, A., Volodin, E., Wyser, K., Xin, X., Yang, S., Yu, Y., Ziehn, T., 2021. Climate model projections from the scenario model intercomparison project (ScenarioMIP) of CMIP6. Earth Syst. Dyn. 12 (1), 253–293. https://doi.org/10.5194/esd–12–253–2021.
Turner, A.K., Hunke, E.C., 2015. Impacts of a mushy–layer thermodynamic approach in global sea–ice simulations using the CICE sea–ice model. J. Geophys. Res. Ocean 120 (2), 1253–1275. https://doi.org/10.1002/2014JC010358.
Wang, B., Zhou, X., Ding, Q., Liu, J., 2021. Increasing confidence in projecting the Arctic ice–free year with emergent constraints. Environ. Res. Lett. 16 (9), 094016 https://doi.org/10.1088/1748–9326/ac0b17.
Wang, H., Zhang, L., Chu, M., Hu, S., 2020. Advantages of the latest los alamos sea–ice model (CICE): evaluation of the simulated spatiotemporal variation of Arctic sea ice. Atmos. Ocean. Sci. Lett. 13 (2), 113–120. https://doi.org/10.1080/16742834.2020.1712186.
Wei, T., Yan, Q., Qi, W., Ding, M., Wang, C., 2020. Projections of Arctic sea ice conditions and shipping routes in the twenty–first century using CMIP6 forcing scenarios. Environ. Res. Lett. 15 (10), 104079 https://doi.org/10.1088/1748–9326/abb2c8.
Weijer, W., Cheng, W., Garuba, O.A., Hu, A., Nadiga, B.T., 2020. CMIP6 models predict significant 21st century decline of the Atlantic meridional overturning circulation. Geophys. Res. Lett. 47 (12), e2019GL086075 https://doi.org/10.1029/2019GL086075.
Winton, M., 2011. Do climate models underestimate the sensitivity of Northern Hemisphere sea ice cover? J. Clim. 24, 3924–3934. https://doi.org/10.1175/2011JCLI4146.1.
Yu, L., Liu, J., Gao, Y., Shu, Q., 2022. A sensitivity study of Arctic ice–ocean heat exchange to the three–equation boundary condition parametrization in CICE6. Adv. Atmos. Sci. 39, 1398–1416. https://doi.org/10.1007/s00376–022–1316–y.
Zhang, M.Z., Xu, Z., Han, Y., Guo, W., 2022. Evaluation of CMIP6 models toward dynamical downscaling over 14 CORDEX domains. Clim. Dyn. https://doi.org/10.1007/s00382–022–06355–5.
Zunz, V., Goosse, H., Massonnet, F., 2013. How does internal variability influence the ability of CMIP5 models to reproduce the recent trend in Southern ocean sea ice extent? Cryosphere 7 (2), 451–468. https://doi.org/10.5194/tc–7–451–2013.